Journal of Applied Polymer Science

Fabrication and characterization of maleic anhydride grafted polypropylene membranes with high antifouling properties

Nader Jahanbakhshi, Seyyed Abbas Mousavi, Fathollah Farhadi
Department of Chemical and Petroleum Engineering, Sharif University of Technology, Azadi Avenue, P.O. Box 11155 9465, Tehran, Iran
Correspondence to: S. A. Mousavi (E-mail: musavi@sharif.edu)

ABSTRACT: In this study, maleic anhydride grafted polypropylene microporous flat-sheet membranes were prepared via a thermally induced phase separation method with a mixture of dibutyl phthalate and dioctyl phthalate as a diluent. The effects of the polymer composition and coagulation bath temperature on the morphology and performance of the fabricated membranes were investigated. The hydrophilicity results of the membranes demonstrated that membrane modification reduced the water contact angle by about 45°, whereas the pure water flux was enhanced about four times. The antifouling behavior of the fabricated membranes was also investigated in a membrane bioreactor. The results show that the pure water flux, membrane pore size, and porosity decreased, whereas the antifouling performance was improved with increasing polymer concentration and decreasing bath temperature. Finally, the results reveal that the removal efficiency of contaminates was independent on the membrane characterization and was done exclusively through biological removal. © 2016 Wiley Periodicals, Inc. J. Appl. Polym. Sci. **2016**, *133*, 43857.

KEYWORDS: bioengineering; grafting; membranes

Received 23 October 2015; accepted 27 April 2016
DOI: 10.1002/app.43857

INTRODUCTION

Polypropylene (PP) is a commonly used polymer in membrane preparation. This is because of its excellent properties, such as its low cost, good mechanical properties, thermal stability, and chemical resistance.[1–6] Despite these outstanding properties, the nonpolar structure of the PP membrane limits its application in aqueous solution separation and membrane bioreactor (MBR) processes. In general, because of the hydrophobic interaction between the membrane, solutes, and microbial cells, hydrophobic membranes such as PP membranes have a higher fouling tendency than hydrophilic ones.[7,8] Therefore, to reduce PP membrane fouling, many efforts have been made to hydrophilically modify these membranes.[9–13]

Yu and coworkers used modified PP microporous membranes via O_2,[14] CO_2,[15] NH_3,[16] and air plasma treatment[17] to improve their antifouling properties in submerged membrane bioreactors. Their results show that the filtration performance and fouling were improved by membrane modification in submerged membrane bioreactors. Their results also demonstrate that CO_2 plasma had the best antifouling behavior.[17] Xie *et al.*[18] used the physical adsorption of Tween 20 on PP microporous membranes to improve the fouling-resistance properties in an MBR. The results show that the adsorption of Tween 20 onto the hydrophobic PP microporous membrane not only enhanced the hydrophilic action but also improved the antifouling ability in an MBR. Yang *et al.*[19] considerably enhanced the surface hydrophilicity of PP membranes through grafting with poly(sulfobetaine methacrylate), where the water contact angle decreased from 145° to approximately 15° and the water flux increased four times. Zhao *et al.*[20] improved the antifouling properties of PP membranes by surface grafting with a zwitterionic polymer, [3-(methacryloylamino)propyl] dimethyl(3-sulfopropyl) ammonium hydroxide. Their results show that a water flux recovery (FR) ratio as high as 90% was achieved for the modified membranes, whereas it was only about 30% for the neat membrane. All of the PP membranes used in MBR are microfiltration membranes. Also, to the best of our knowledge, there have been no investigations on the application of PP ultrafiltration membranes in MBR.

To modify the PP membrane, many materials are grafted on the PP surface, but maleic anhydride grafted polypropylene (PP-*g*-MA) is one of the most important and commercial amphiphilic polymers.[21] The introduction of polar groups of maleic anhydride (MA) to the main chains of PP (Figure 1) improved the PP membrane performance. Saffar *et al.*[21] prepared a hydrophilic microporous membrane via a melt-extrusion technique with a blending method with PP-*g*-MA and acrylic acid grafted PP. Their results show that the solubility of water in the

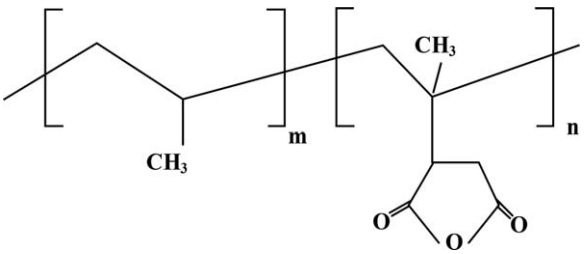

Figure 1. Chemical structure of PP-*g*-MA.

polymers was enhanced by the addition of these amphiphilic copolymers.

To our knowledge so far, there has been no study on the effect of MA on PP membrane antifouling properties. In this research, ultrafiltration flat membranes were prepared via a thermally induced phase separation (TIPS) technique with PP-*g*-MA as a hydrophilic polymer and the mixture of dioctyl phthalate (DOP)/dibutyl phthalate (DBP) as a diluent. Then, the fabricated ultrafiltration membranes were examined to investigate the effect of the initial polymer concentration and coagulation bath temperature on the membrane performance. In addition, the effect of MA on the membrane properties was studied, and the obtained results show significant improvements in the water permeation and antifouling properties. Finally, the prepared membranes were also used in MBR to investigate membrane fouling during the membrane filtration of activated sludge.

EXPERIMENTAL

Flat-Sheet Membrane Preparation

PP-*g*-MA (Ariapolymer Co, Iran) as a polymer and mixture of DBP/DOP (Aekyung Petrochemical Co., Korea) as a diluent were added to a vessel, whereas the mass ratio of DOP to DBP was kept constant at 1.22. The mixture of polymer and diluent was heated and stirred at 200 °C for 2 h until a homogeneous solution was obtained. The homogeneous solution was cast over a preheated glass plate with a thickness of 150 μm and then submerged in a water bath for 10 min. When the thermal phase separation took place, the porous structure was formed. The diluents were extracted by immersion of the fabricated membranes into ethanol. Finally, to completely remove the diluents and water, the fabricated membranes were dried.

Membrane Characterization

Porosity and Pore Size Measurements. To obtain the membrane porosity, the dry weight of the membranes was measured. The membranes were immersed in ethanol for 24 h to wet them, and then, they were immediately weighed after ethanol was removed from the surface. The porosity of the membranes (A_k) was calculated according to the following formula[22]:

$$A_k = \frac{(w_2 - w_1)\rho_1}{\rho_1 w_1 + (\rho_2 - \rho_1) w_1} \times 100\% \quad (1)$$

where w_1 is the initial membrane weight, w_2 is the immersed membrane weight, and ρ_1 and ρ_2 are the densities of PP-*g*-MA (0.91 g/cm^3) and ethanol (0.8 g/cm^3), respectively.

Guerout–Elford–Ferry equation was used to determine the mean pore radius [r_p (mm)][23,24]:

$$r_p = \sqrt{\frac{(2.9 - 1.75\varepsilon) 8\eta l \dot{Q}}{\varepsilon A \Delta P}} \quad (2)$$

where η is the water viscosity (0.001 Pa s), l is the membrane thickness (m), $\dot{Q}$ is the volumetric flow rate (m^3 s^{-1}), A is the effective membrane area (m^2), ε is the membrane porosity, and ΔP is the operational pressure (0.048 MPa).

Pure Water Flux. Before the pure water flux measurements were done, the PP-*g*-MA membranes were prewetted by immersion into ethanol for more than 24 h. Membranes with an effective area of 12.56 cm^2 were initially precompacted with distilled water at 60 kPa for 20 min. After compaction, the pure water flux of the membranes was measured at a fixed transmembrane pressure of 48 kPa until the consecutive five recorded values differed by less than 2%. The water flux was calculated with the following equation:

$$J_0 = \frac{Q}{At} \quad (3)$$

where J_0 is the deionized water flux (L m^{-2} h^{-1}), Q is the volume of collected permeate (L), and t is the reaction time (h), respectively. Three trials were performed for each sample, and the average values are reported as the permeability of each type of flat-sheet membrane.

Mechanical Properties. The mechanical properties of membranes were measured on the films with a universal testing machine (HIWA 2126, Iran). Every test was carried out at room temperature and according to ASTM D 3039. Each sample was clamped at both ends with a rectangular geometry 10 mm wide and 40 mm long and was then stretched at a crosshead speed of 2 mm/min. Three trials were performed for each sample, and the average values are reported.

Scanning Electron Microscopy (SEM). A KYKY-EM3200 digital scanning electron microscope (China) with an accelerating voltage of 24 kV was used to observe the membrane morphology. To observe the membrane cross sections, the prepared PP-*g*-MA membranes were frozen and broken in liquid nitrogen; then, their cross sections were sputtered with gold–palladium.

Filtration Experiments

The MBR (Figure 2) with dimensions of 60, 22, and 6.5 cm was used. The effective area of the prepared membranes was 12.56 cm^2. To supply the required oxygen for biological processes and to reduce the fouling rate, the aeration process was done in MBR. The aerobic sludge used in the MBR basin was supplied from the activated sludge of Tabriz Petrochemical Co. and was then adapted with the synthetic feed for 1 month. For this purpose, the initial influent styrene and ethylbenzene concentrations were set to about 10 mg/L and then increased to 100 mg/L with a few step changes for 1 month. Also, the air rate, temperature, and feed rate were 6 L/min, 25 °C, and 0.5 L/h, respectively. The operating conditions are reported in Table I.

The synthetic wastewater used in this research was formulated to simulate petrochemical industrial wastewater in terms of the chemical oxygen demand (COD), styrene, and ethylbenzene concentrations, which were 1200, 100, and 100 mg/L, respectively. Ethanol was used as a carbon source and created a COD

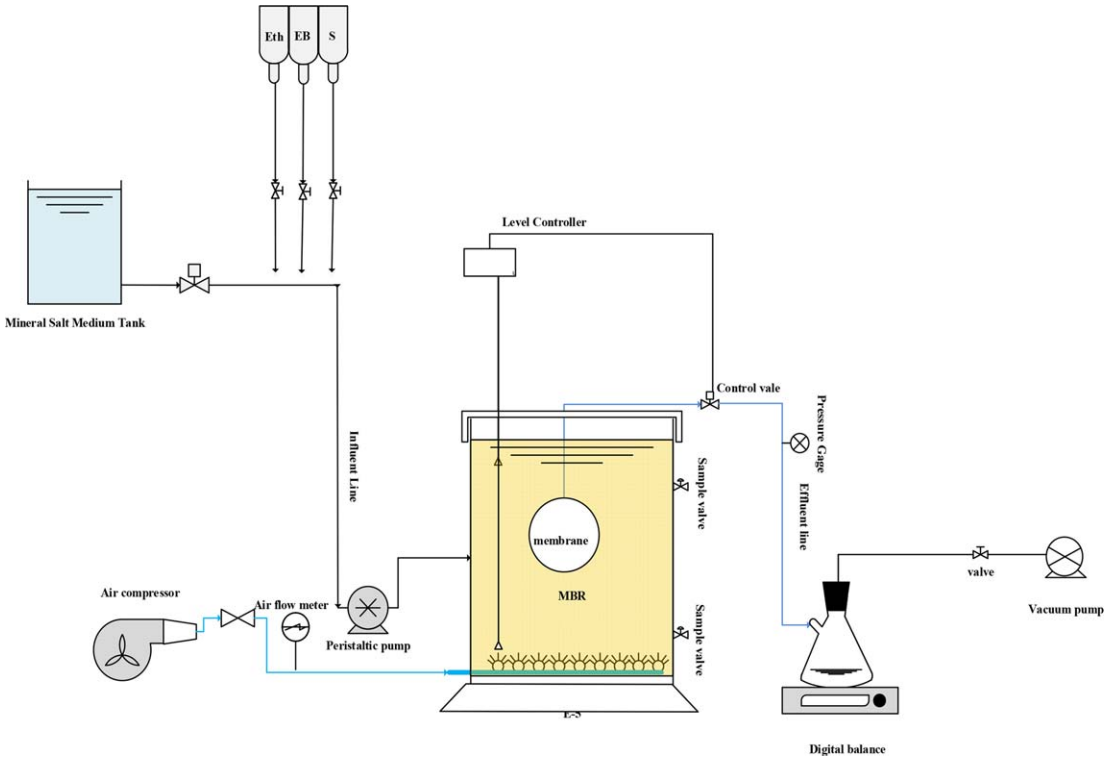

Figure 2. Scheme of the experimental setup. EB = ethyl benzene; Eth = ethanol; S = styrene. [Color figure can be viewed in the online issue, which is available at www.interscience.wiley.com.]

concentration of about 1200 mg/L. Moreover, to prevent the volatile organic compounds (VOCs) from stripping to air from the feed, the VOCs were separately injected into the feed stream. To ensure that the influent VOC and COD concentrations did not decrease, these parameters were analyzed periodically. The compositions of the synthetic wastewaters are reported in Table II.

The styrene and ethylbenzene concentrations were analyzed with a gas chromatograph (Young Lin, ACME-6100). The styrene and ethylbenzene concentrations in the liquid phase were estimated with the headspace method.[25] The gas flow rate from the bioreactor headspace was measured with a flow meter. The mixed-liquor-suspended solids and COD were estimated according to standard methods.[26]

Table I. Operating Conditions of the MBR

Hydraulic retention time (h)	15
Solid retention time (days)	20
Dissolved oxygen (mg of O_2/L)	3–4
Mixed liquor suspended solids (mg/L)	4000–5000
pH	7.0 ± 0.2
Feed concentration (mg of COD/L)	1200
Air flow rate (L/min)	6
Transmembrane pressure (mmHg)	360
Working volume (L)	7
Temperature (°C)	Room temperature

Membrane Fouling Analysis

During the operation in the MBR, the flux curve was measured under 48 kPa for each sample. At the end of the process, the final permeation flux (J_p) was calculated. After continuous operation and cake layer formation, the membrane surface was cleaned with pure water, and then, the pure water flux (J_1) was measured. The antifouling characteristics, such as FR and the fouling index (FI), were obtained from the following equations[7,9,14]:

Table II. Composition of the Synthetic Wastewater

Component	Concentration (mg/L)
Ethanol	370
Styrene	100
Ethylbenzene	100
NH_4Cl	560
K_2HPO_4	35
KH_2PO_4	45
$MgSO_4{\cdot}7H_2O$	13
$CaCl_2{\cdot}2H_2O$	7
$FeCl_3$	5
$ZnSO_4$	2
$NaHCO_3$	500
Ethylene diamine tetraacetic acid ($C_{10}H_{16}N_2O_8$)	7

$$FR = \frac{J_1}{J_0} \quad (4)$$

$$FI = 1 - \frac{J_P}{J_0} \quad (5)$$

To calculate the characteristics of membrane fouling, the resistance-in-series model was used.[27] According to this model, the flux and membrane resistances were obtained by the following equations[15]:

$$J = \frac{\Delta P_T}{\eta R} \quad (6)$$

$$R_t = R_m + R_r + R_{ir} \quad (7)$$

$$R_m = \frac{\Delta P_T}{\eta J_0} \quad (8)$$

$$R_t = \frac{\Delta P_T}{\eta J_P} \quad (9)$$

$$R_{ir} = \frac{\Delta P_T}{\eta J_1} - R_m \quad (10)$$

$$R_r = \frac{\Delta P_T}{\eta J_p} - R_m - R_{ir} \quad (11)$$

where J is the permeate flux (L m^{-2} h^{-1}), ΔP_T (48 kPa) is the transmembrane pressure, η is the viscosity of the permeate, R_t is the total membrane fouling resistance (m^{-1}), R_m is the inherent membrane resistance (m^{-1}), R_r is the reversible fouling resistance or cake resistance (m^{-1}), and R_{ir} is the irreversible fouling resistance or pore resistance (m^{-1}).

RESULTS AND DISCUSSION

Membrane Performance

In the TIPS technique, the effects of the initial polymer concentration and the quenching bath temperature on the membrane structure are vital parameters because the phase separation mechanism can be changed with the concentration and temperature.[28] The morphology of the PP-*g*-MA membrane is influenced by the polymer concentration and quenching temperature. The cross-sectional morphologies of the PP-*g*-MA membranes at various polymer concentrations and a bath temperature of 45 °C are given in Figure 3. As shown in this figure, the prepared membrane pore size decreased with increasing PP-*g*-MA concentration. In the TIPS technique, the porous structure is related to the presence of the polymer-lean phase, and this phase forms the membrane pores. Therefore, when the polymer weight percentage is increased, the diluent weight fraction and volume fraction of the polymer-lean phase is reduced, so there are not enough diluents for extraction, and subsequently, the membrane pore size and porosity decrease.

The porosity, mean pore size, and tensile strength values of the membranes at different concentrations of PP-*g*-MA and at a bath temperature of 45 °C are listed in Table III. Because of the decreasing fraction of the polymer-lean phase with increasing the initial polymer concentration, the membrane porosity and pore size decreased. These results are consistent with the SEM cross-sectional images (Figure 3). Table III shows that the pure water flux decreased with increasing polymer concentration. This could be explained by the enhancement of the membrane resistance against water permeation through the membrane with decreasing membrane pore size and porosity. Table III also shows that the polymer concentration had positive effects on the membrane mechanical properties. This was probably due to the reduction of the polymer-lean phase growth and the more compact structure in the prepared membranes at high concentrations of the polymer.

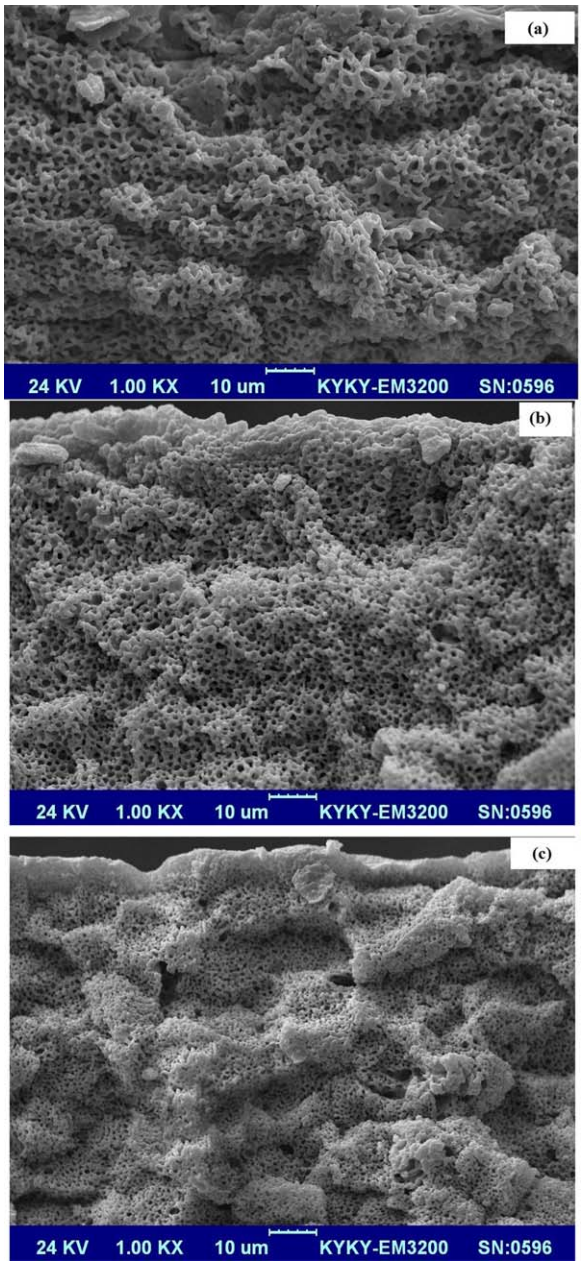

Figure 3. Micrographs of the cross sections of the PP-*g*-MA membranes at a coagulation bath temperature of 45 °C and at polymer concentrations of (a) 20, (b) 25, and (c) 30 wt %. [Color figure can be viewed in the online issue, which is available at www.interscience.wiley.com.]

The porosity, mean pore size, and tensile strength of the membranes and the pure water flux results at different quenching temperatures and at a polymer concentration of 25 wt % are listed in Table IV. As shown in this table, with increasing bath

Table III. Values of the Membrane Porosity, Pore Size, Tensile Strength, and Hydraulic Permeability at a Bath Temperature of 45 °C

PP-*g*-MA (wt %)	Porosity		Mean pore size		Tensile strength		Pure water flux	
	Value (%)	Error (%)	Value (μm)	Error (%)	Value (MPa)	Error (%)	Value (L m^{-2} h^{-1})	Error (%)
20	66	±5.3	0.051	±3.9	0.92	±4.7	140	±4.8
25	58	±1.2	0.048	±2.2	1.44	±2	100	±6
30	55	±1	0.047	±1.8	1.84	±5	88	±5.3

The errors are the percentage errors of duplicate experiments.

temperature from 30 to 60 °C, the pure water flux increased from 71 to 135 L m^{-2} h^{-1}; this was due to the increasing membrane porosity and pore size. The increase in the bath temperature led to a decrease in the supercooling degree and, subsequently, to the slower solidification rate of the polymer-rich phase. This phenomenon provided a long time for the polymer-lean phase to grow and caused an increase in the final membrane pore size and porosity.

Table IV also reveals that with increasing membrane porosity, the tensile strength decreased. The more compact structure in the prepared membranes at lower bath temperatures was also confirmed by the SEM cross-sectional photos, which are shown in Figure 4.

Effect of MA Grafting on the PP Membrane Performance

To evaluate the effect of MA grafting into the PP membranes, the pure water flux for both the PP and PP-*g*-MA membranes were measured and are illustrated in Figure 5. The results indicate the significant influence of MA grafting into PP; it effectively improved the performance of the PP membranes. These results were attributed to the presence of polar groups in the membrane structure and the increase in the membrane pore size. The presence of polar groups in the modified PP membrane structure and the formation of hydrogen bonds with water molecules enhanced the hydrophilicity of the PP membranes.[21] This result was verified by contact angle measurements (Figure 6). The contact angle data indicated that the water contact angle decreased from 139° for the neat membranes to 93° for the modified ones. Moreover, as shown in Figure 7, the modified membranes had larger pore sizes than the neat ones. Membrane modification decreased the compatibility of PP–DOP/DBP; subsequently, the two-phase region shifted toward higher temperatures, and the phase separation region became wider.[29,30] The increase in the separation region provided a longer time for pore growth, and this led to larger pore sizes (Table V). Therefore, the presence of polar groups and larger pore sizes increased the water flux.

To investigate the antifouling properties of the neat and modified membranes, filtration experiments of activated sludge in an MBR were performed. The synthetic wastewater permeate flux results for the prepared membranes at a polymer concentration of 25 wt % and a bath temperature of 45 °C for the neat and modified PP membranes are shown in Figure 8. As shown in this figure, both membranes had a similar trend in the decline of the permeate flux. However, the modified PP membrane, because it had polar groups in its structure and a large pore size, had a higher flux.

FI and FR, which are reported in Table VI, showed that the modified PP membrane had a better performance. This was probably related to the lower contaminant adsorption on the hydrophilic membrane.[15] Pore fouling is affected by three characteristics of membranes: structure, pore size, and hydrophilicity. Pore fouling decreases with decreasing membrane pore size and increasing hydrophilicity.[31] R_m in a modified membrane is reduced by 80% because of membrane modification, whereas Yu[15] reduced R_m by only 28% via surface modification. This was probably related to the presence of polar groups in the bulk structure instead of the membrane surface. The lower value of R_r in the PP-*g*-MA membrane was related to the lower impact tendency of the pollutant on the hydrophilic membrane surface and their more easy elimination from the membrane surface.[15] The results also show that R_t significantly decreased with membrane modification and the subsequent decreases in R_m and R_r.

Membrane Fouling Evaluation

Flux Decline. To study the effect of the initial polymer concentration and coagulation bath temperature on membrane fouling, filtration experiments of activated sludge in an MBR were carried out. Figures 9 and 10 show the permeate variations during the filtration experiments for different membranes. As indicated in these figures, a similar trend was observed for all of the

Table IV. Values of the Membrane Porosity, Pore Size, Tensile Strength, and Hydraulic Permeability at the Polymer Concentration of 25 wt %

Bath temperature (°C)	Porosity		Mean pore size		Tensile strength		Pure water flux	
	Value (%)	Error (%)	Value (μm)	Error (%)	Value (MPa)	Error (%)	Value (L m^{-2} h^{-1})	Error (%)
30	47	±4.7	0.046	±2.1	1.54	±3.7	71	±6.7
45	58	±1.2	0.048	±2.2	1.44	±2	100	±6
60	65	±2.3	0.050	±1	1.28	±4	135	±5.3

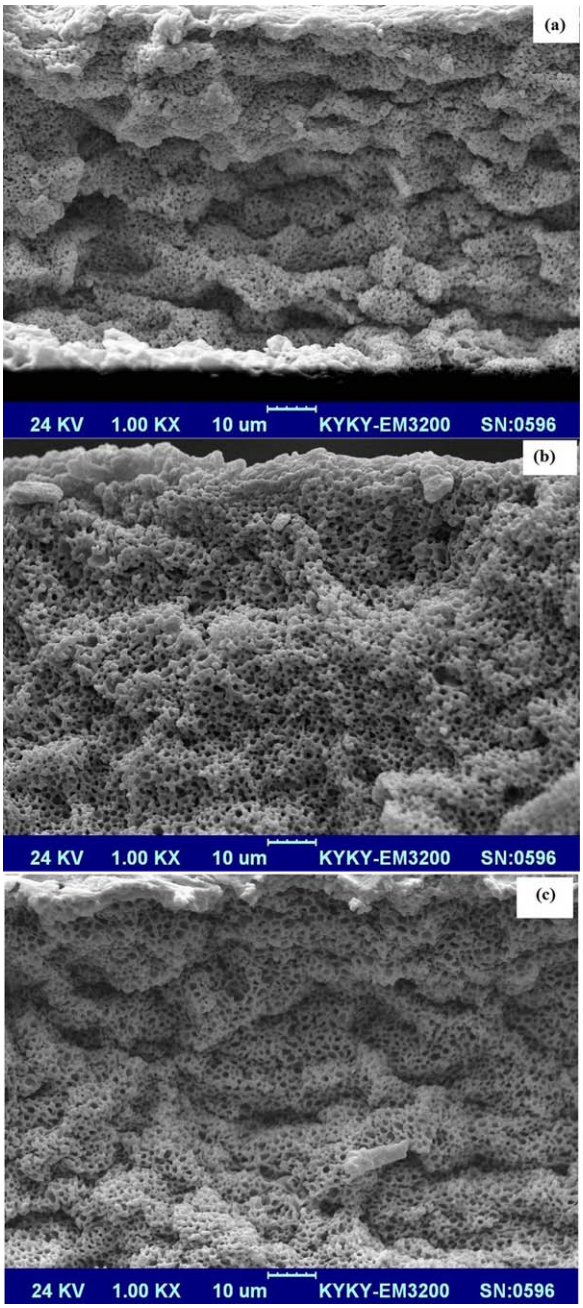

Figure 4. Micrographs of the cross sections of the PP-*g*-MA membranes at a polymer concentration of 25 wt % and at bath temperatures of (a) 30, (b) 45, and (c) 60 °C. [Color figure can be viewed in the online issue, which is available at wileyonlinelibrary.com.]

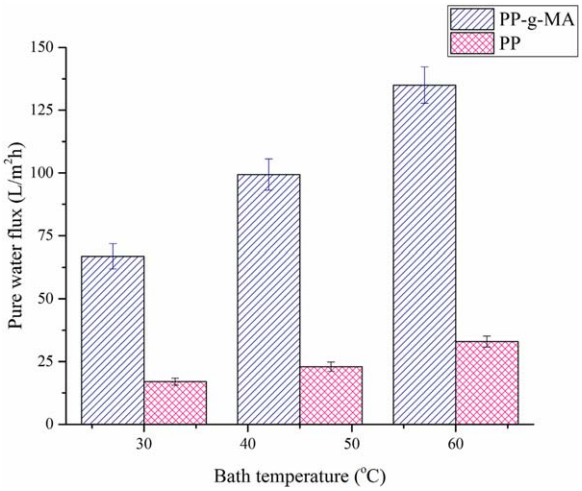

Figure 5. Effect of MA grafting on the PP membrane performance. The error bars represent the data range of duplicate samples. [Color figure can be viewed in the online issue, which is available at wileyonlinelibrary.com.]

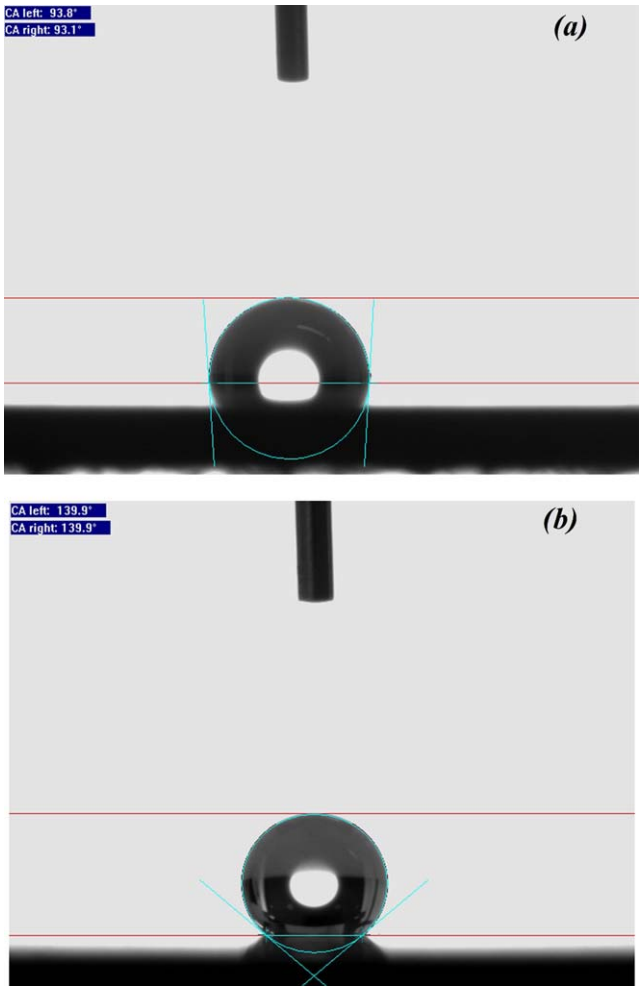

Figure 6. Contact angle (CA) values for the (a) modified and (b) neat membranes. [Color figure can be viewed in the online issue, which is available at wileyonlinelibrary.com.]

membranes. Moreover, in all cases, the synthetic wastewater permeate flux declined rapidly within the initial times of filtration. This was probably related to the increase in the membrane resistance because of membrane pore blocking. After this rapid reduction in the permeate flux, because of cake formation, the flux decline continued with a gentle slope until a constant value was reached.

SEM images of the membrane surface and cross section after the filtration of activated sludge in an MBR are shown in

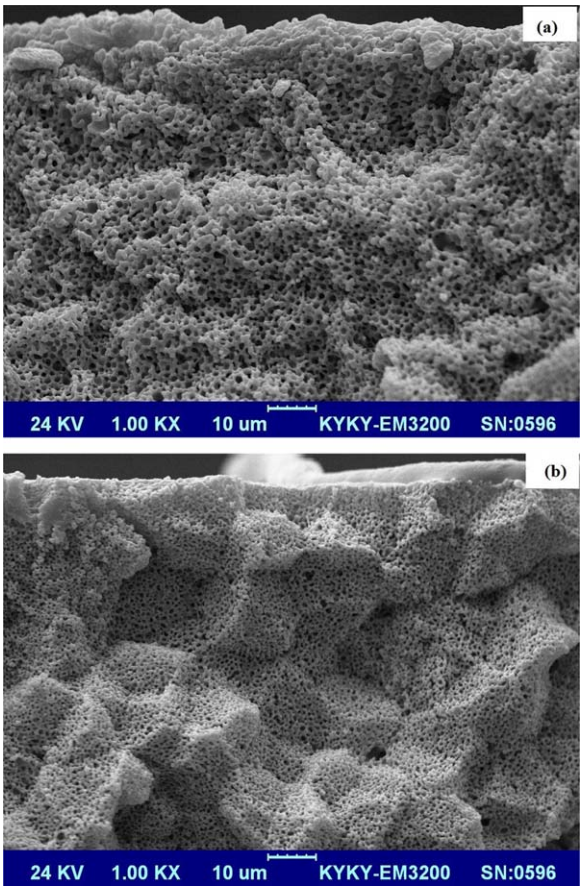

Figure 7. Micrographs of the cross sections of the (a) PP-*g*-MA membrane and (b) PP membrane at a polymer concentration of 25 wt % and a bath temperature of 45 °C. [Color figure can be viewed in the online issue, which is available at wileyonlinelibrary.com.]

Figure 11. The thickness of the cake was about 3 μm. As shown in this figure, the surface of the cake was uneven, and the structure was very compact.

Figures 9 and 10 also show that the PP-g-MA membranes with the lowest pore size had the lowest permeate flux. This means that these membranes could eliminate the small size particles. Subsequently, this led to the formation of cakes with a more compact structure and more resistance to water permeation.

The calculated FI and FR values of the PP-*g*-MA membrane are reported in Table VII. The results show that with decreasing bath temperature and increasing polymer concentration, FI decreased. The decrease in the membrane pore size and porosity due to the increase in the polymer concentration and decrease in the bath temperature decreased the membrane pore blocking and subsequently FI. This also means that the constant fouling on the membranes decreased with decreasing membrane pore size. According to the results presented in Table VII, we concluded that the lowest (68%) and highest (81%) FIs were obtained for the prepared membranes at experimental conditions corresponding to 25 wt % and 30 °C and 20 wt % and 45 °C, respectively. After membrane washing and the removal of the cake layer, an excellent fouling recovery (41%) was obtained for the prepared membranes for experimental condition 4. This condition corresponded to the membrane with lowest value of FI. This indicated that this membrane had better performance because of the lower value of FI and the higher value of FR.

Table V. Mean Membrane Pore Size at the Polymer Concentration of 25 wt %

Bath temperature (°C)	PP-*g*-MA		PP	
	Value (μm)	Error (%)	Value (μm)	Error (%)
30	0.046	±2.1	0.022	±1.7
45	0.048	±2.2	0.023	±1.5
60	0.050	±1	0.025	±1.1

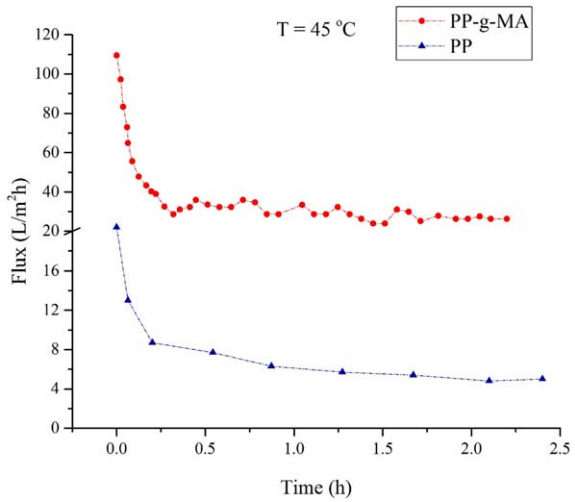

Figure 8. Synthetic wastewater permeate flux decline for the modified and neat membranes. *T* = bath temperature. [Color figure can be viewed in the online issue, which is available at wileyonlinelibrary.com.]

Yu *et al.*[17] reported that the FRs after water cleaning were 37, 12.3, 23, and 22.69% for CO_2, O_2, NH_3, and air plasma treatment membranes with an average pore size of 0.10 μm, whereas the FR for the PP-*g*-MA membranes at the best condition was 41%. These results demonstrate that PP modification with MA enhanced FR. However, the membrane pore size was probably effective, as shown by the obtained results.

The R_m, R_r, R_{ir}, and R_t values for each membrane were calculated and are reported in Table VIII. The results demonstrate that with increasing polymer concentration and decreasing bath temperature, R_m increased. As mentioned before, the enhancement of the membrane resistance was due to the decrease in the membrane

Table VI. Antifouling Properties and Resistance Values for the Modified and Neat Membranes

Membrane	FI (%)	FR (%)	Resistance ($\times 10^{14}$ m^{-1})			
			R_m	R_t	R_r	R_{ir}
PP-*g*-MA	73	39	5.7	21.2	8.9	6.6
PP	77	35	28	123	54	42

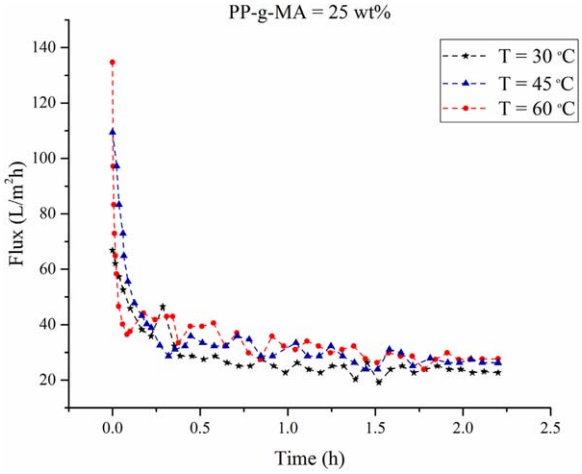

Figure 9. Synthetic wastewater permeate flux decline at a transmembrane pressure of 48 kPa for bath temperature (T) values of 30, 45, and 60 °C. [Color figure can be viewed in the online issue, which is available at wileyonlinelibrary.com.]

pore size and porosity. Similar results were obtained with the Hagen–Poiseuille equation.[32,33] The R_{ir} results reveal that membranes with lower pore sizes and porosities had lower R_{ir} values. These results were consistent with the results of fouling. The measured R_r indicated that the cake layer resistance played a significant role in membrane fouling,[7] and R_r had the largest share of R_t. The consideration of the values of R_r accompanied by the permeate flux results revealed that the higher values of R_r in the membrane with a lower pore size must have been related to the cake density. Particles with a small size, which could not pass through the membranes with smaller pore sizes, provided a cake with a higher density and, subsequently, a higher value of R_r.

COD, Styrene, and Ethylbenzene Removal Efficiencies. Activated sludge removes VOCs through stripping, adsorption, and biodegradation. According to previous studies,[34] the contribution of

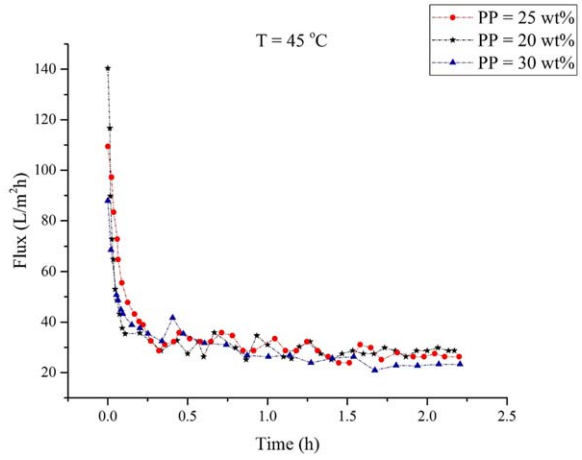

Figure 10. Permeate flux decline at a transmembrane pressure of 48 kPa for polymer concentrations of 20, 25, and 30 wt %. T = bath temperature. [Color figure can be viewed in the online issue, which is available at wileyonlinelibrary.com.]

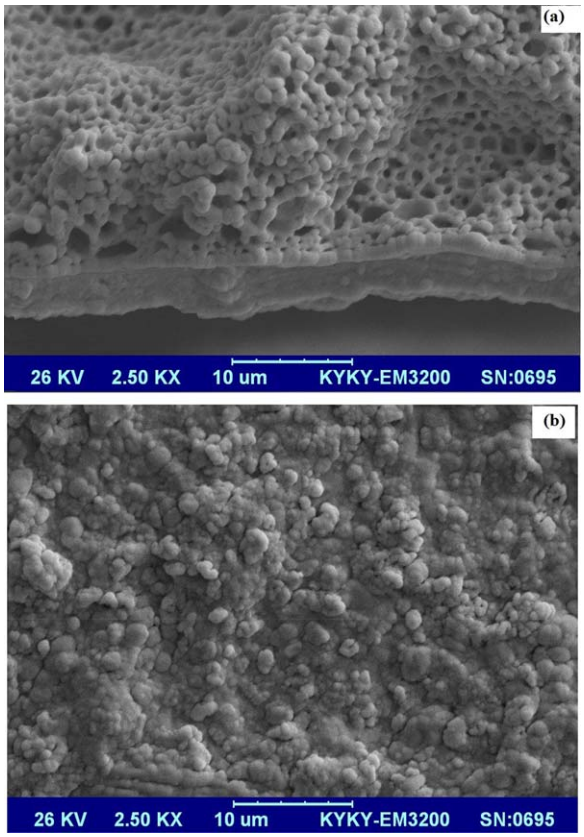

Figure 11. Micrographs of the (a) cross section and (b) surface of the PP-*g*-MA membrane at a polymer concentration of 25 wt % and a bath temperature of 45 °C. [Color figure can be viewed in the online issue, which is available at wileyonlinelibrary.com.]

the adsorption mechanism by activated sludge for styrene and ethylbenzene is not very substantial. Therefore, we assumed that the overall removal efficiency for styrene and ethylbenzene was through biological and stripping removal. The overall removal efficiencies of COD, styrene, and ethylbenzene in an MBR are reported in Table IX for all of the membranes.

The removal efficiency for COD was from 92 to 98%, and those for for ethylbenzene and styrene were more than 99% in steady-state conditions. The results show that the removal efficiency

Table VII. Antifouling Properties of the Fabricated Membranes

	Membrane preparation			
Experiment	PP-*g*-MA (wt %)	Temperature (°C)	FI (%)	FR (%)
1	20	45	81	31
2	25	45	73	39
3	30	45	73	35
4	25	30	68	41
5	25	45	73	39
6	25	60	80	28

Table VIII. Filtration Resistances of the Fabricated Membranes

	Membrane preparation		Resistance ($\times 10^{14}$ m^{-1})				Resistance ratio (%)		
Experiment	PP-*g*-MA (wt %)	Temperature (°C)	R_m	R_t	R_{ir}	R_r	R_m/R_t	R_{ir}/R_t	R_r/R_t
1	20	45	4.4	23.7	9.5	9.8	19	40	41
2	25	45	5.7	21.2	6.6	8.9	27	31	42
3	30	45	7.0	26.6	6.4	13.1	26	24	49
4	25	30	8.8	27.4	5.9	12.7	32	21	46
5	25	45	5.7	21.2	6.6	8.9	27	31	42
6	25	60	4.6	23.6	6.9	12.1	20	29	51

Table IX. COD, Styrene, and Ethylbenzene Removal Efficiency for the Fabricated Membranes

			Removal efficiency (%)			
Experiment	PP-*g*-MA (wt %)	Temperature (°C)	COD	Ethylbenzene and styrene (permeate)	Ethylbenzene (exit air)	Styrene (exit air)
1	20	45	95	99.9	0.9	2.2
2	25	45	98	99.9	1.5	2.8
3	30	45	92	99.9	0.5	1.3
4	25	30	96	99.9	1	1.6
5	25	45	98	99.9	1.5	2.8
6	25	60	94	99.9	2	3

was independent of the membrane characterization, and contaminant removal efficiency for all of the membranes was desirable. We, therefore, concluded that the removal efficiency depended on the sludge biological properties and was not related to structures of the membrane. The ethylbenzene and styrene concentrations in the reactor exit air were measured and are reported. The results show that the range of removal efficiencies thorough a stripping mechanism for ethylbenzene and styrene were 0.5 to 2% and 1.3 to 3%, respectively. We, therefore, concluded that the stripping mechanism did not contribute to the removal of styrene and ethylbenzene during the operation at the reactor. Therefore, we deduced that during the MBR processes, the styrene and ethylbenzene removal were exclusively through biological removal.

CONCLUSIONS

The PP-*g*-MA flat-sheet membranes were prepared via a TIPS technique and used in an MBR to investigate the membrane antifouling performance. The effects of the preparation conditions on the morphology and performance of the fabricated membranes showed that with increasing polymer concentration and decreasing bath temperature, the membrane porosity, pore size, and pure water flux decreased, whereas the membrane mechanical properties increased. The filtration results also show that the membrane fouling increased with increasing bath temperature and decreasing polymer concentration. Moreover, the overall removal efficiency of COD, styrene, and ethylbenzene exhibited that the removal efficiency was independent of the membrane characterization. Finally, the hydrophilic modification of the membranes improved the filtration performance and antifouling properties.

REFERENCES

1. Jones, T. D.; Chaffin, K. A.; Bates, F. S.; Annis, B.; Hagaman, E.; Kim, M.-H.; Wignall, G. D.; Fan, W.; Waymouth, R. *Macromolecules* **2002**, *35*, 5061.
2. Matsuyama, H.; Maki, T.; Teramoto, M.; Asano, K. *J. Membr. Sci.* **2002**, *204*, 323.
3. Luo, B.; Li, Z.; Zhang, J.; Wang, X. *Desalination* **2008**, *233*, 19.
4. Lin, Y.; Chen, G.; Yang, J.; Wang, X. *Desalination* **2009**, *236*, 8.
5. Matsuyama, H.; Yuasa, M.; Kitamura, Y.; Teramoto, M.; Lloyd, D. R. *J. Membr. Sci.* **2000**, *179*, 91.
6. Matsuyama, H.; Kim, M.-M.; Lloyd, D. R. *J. Membr. Sci.* **2002**, *204*, 413.
7. Yu, H.-Y.; Xu, Z.-K.; Yang, Q.; Hu, M.-X.; Wang, S.-Y. *J. Membr. Sci.* **2006**, *281*, 658.
8. Kim, D. S.; Kang, J. S.; Lee, Y. M. *Sep. Sci. Technol.* **2005**, *39*, 833.
9. Yu, H.-Y.; Xu, Z.-K.; Xie, Y.-J.; Liu, Z.-M.; Wang, S.-Y. *J. Membr. Sci.* **2006**, *279*, 148.
10. Wavhal, D. S.; Fisher, E. R. *Langmuir* **2003**, *19*, 79.

11. Belfer, S.; Fainshtain, R.; Purinson, Y.; Gilron, J.; Nyström, M.; Mänttäri, M. *J. Membr. Sci.* **2004**, *239*, 55.
12. Liu, L.; Liu, J.; Bo, G.; Yang, F.; Crittenden, J.; Chen, Y. *J. Membr. Sci.* **2013**, *429*, 252.
13. Guo, H.; Ulbricht, M. *J. Membr. Sci.* **2010**, *349*, 312.
14. Yu, H. Y.; He, X. C.; Liu, L. Q.; Gu, J. S.; Wei, X. W. *Plasma Process. Polym.* **2008**, *5*, 84.
15. Yu, H.-Y.; Xie, Y.-J.; Hu, M.-X.; Wang, J.-L.; Wang, S.-Y.; Xu, Z.-K. *J. Membr. Sci.* **2005**, *254*, 219.
16. Yu, H.-Y.; Hu, M.-X.; Xu, Z.-K.; Wang, J.-L.; Wang, S.-Y. *Sep. Purif. Technol.* **2005**, *45*, 8.
17. Yu, H.-Y.; Liu, L.-Q.; Tang, Z.-Q.; Yan, M.-G.; Gu, J.-S.; Wei, X.-W. *J. Membr. Sci.* **2008**, *311*, 216.
18. Xie, Y.-J.; Yu, H.-Y.; Wang, S.-Y.; Xu, Z.-K. *J. Environ. Sci.* **2007**, *19*, 1461.
19. Yang, Y.-F.; Li, Y.; Li, Q.-L.; Wan, L.-S.; Xu, Z.-K. *J. Membr. Sci.* **2010**, *362*, 255.
20. Zhao, J.; Shi, Q.; Luan, S.; Song, L.; Yang, H.; Shi, H.; Jin, J.; Li, X.; Yin, J.; Stagnaro, P. *J. Membr. Sci.* **2011**, *369*, 5.
21. Saffar, A.; Carreau, P. J.; Ajji, A.; Kamal, M. R. *J. Membr. Sci.* **2014**, *462*, 50.
22. Luo, F.; Zhang, J.; Wang, X.; Chen, J.; Xu, Z. *Acta Polym. Sin.* **2002**, *5*, 566.
23. Li, J.-F.; Xu, Z.-L.; Yang, H.; Feng, C.-P.; Shi, J.-H. *J. Appl. Polym. Sci.* **2008**, *107*, 4100.
24. Sadeghi, I.; Aroujalian, A.; Raisi, A.; Dabir, B.; Fathizadeh, M. *J. Membr. Sci.* **2013**, *430*, 24.
25. Fallah, N.; Bonakdarpour, B.; Nasernejad, B.; Moghadam, M. A. *J. Hazard. Mater.* **2010**, *178*, 718.
26. Clesceri, L. S.; Greenberg, A. E.; Eaton, A. D. Standard Methods for the Examination of Water and Wastewater; American Public Health Association: Washington, DC, **1998**.
27. Mulder, M. Basic Principles of Membrane Technology; Springer: New York, **1996**.
28. Kim, S. S.; Lloyd, D. R. *J. Membr. Sci.* **1991**, *64*, 13.
29. Lloyd, D. R.; Kim, S. S.; Kinzer, K. E. *J. Membr. Sci.* **1991**, *64*, 1.
30. Matsuyama, H.; Teramoto, M.; Kudari, S.; Kitamura, Y. *J. Appl. Polym. Sci.* **2001**, *82*, 169.
31. Fang, H. H.; Shi, X. *J. Membr. Sci.* **2005**, *264*, 161.
32. Shukla, A. A.; Etzel, M. R.; Gadam, S. Process Scale Bioseparations for the Biopharmaceutical Industry; CRC: Boca Raton, FL, **2006**.
33. Baker, R. W. Membrane Technology; Wiley: New York, **2000**.
34. Hsieh, C.-C. *J. Hazard. Mater.* **2000**, *79*, 173.